13th U.S. National Combustion Meeting
Organized by the Central States Section of the Combustion Institute
March 19–22, 2023
College Station, Texas

Optical Characterization of cellular instabilities in spherically expanding ammonia-hydrogen flames

Behlol Nawaz[1,], Md Nayer Nasim[1], Shubhra Kanti Das[1], Dimitris Assanis[2], Juan Pablo Trelles[1], Noah Van Dam[1], and John Hunter Mack[1]*

[1]*Department of Mechanical Engineering, University of Massachusetts Lowell, 1 University Ave, Lowell, MA, USA*
[2]*Department of Mechanical Engineering, Stony Brook University, 113 Light Engineering, Stony Brook, NY, USA*
[*]*Corresponding author:* behlol_nawaz@student.uml.edu

Abstract: Ammonia (NH_3) and hydrogen (H_2) are promising zero-carbon fuels that face numerous technical challenges. Some of the potential issues may be mitigated if they are used together as blends and fundamental combustion studies can provide insight into how these fuels interact. This study aims at improving the understanding of the formation of cellular instabilities as NH_3-H_2 fractions vary at various equivalence ratios. Premixed NH_3-H_2 blends are ignited in a constant volume combustion chamber (CVCC) with optical access and Schlieren images of the resulting spherically expanding flames are recorded using a high-speed camera. The images are processed to automatically determine the length of cracks within the spherical flame and the evolution of instabilities is analyzed using the length of cracks. The mole fraction of H_2 in the H_2/NH_3 blend is varied between 0% and 50% at increments of 10% and the equivalence ratio is varied between 0.5, 0.7, 0.9, 1.0, 1.1, and 1.3 for each mole fraction. It is observed that instabilities appear at shorter flame radii as the fraction of H_2 is increased and the total crack length is also higher. However, this trend diminishes as the equivalence ratio increases and few to no cracks are observed for the richer conditions at high H_2 fractions.

Keywords: ***Ammonia, Hydrogen, Spherical Flames, Image Processing, Instabilities***

1. Introduction

Conventional energy sources are a leading cause of pollution and climate change due to their reliance on fossil fuels. More sustainable alternatives are an active area of research and some technologies are already being adopted on a commercial scale. However, the storage and transmission of renewable energy sources has always been a challenge. Power for transportation, heating, and even electricity is mostly generated from fuels which are easier to handle and transport while possessing a high energy density. Ideal alternatives to conventional fuels would have reduced (or zero) carbon emissions while meeting existing storage and transportation requirements. Ammonia (NH_3) and hydrogen (H_2) are both zero-carbon fuels which come close to meeting these criteria, although their potential usage has several unique challenges. Long-term storage, transportation, and energy conversion from H_2 is challenging due to its explosive nature and tendency to cause metal embrittlement. NH_3, on the other hand, is not as flammable as H_2. It is relatively easier to

store and transport as it does not need as high of pressure and as low temperatures in comparison to H_2. NH_3 already has many applications in existing industries, so it has been widely produced, transported, and used on industrial scales for decades. This is a great advantage as its production, transportation, and storage is well understood at this point. As such, NH_3 has been proposed as both a standalone fuel as well as a carrier for H_2. Most NH_3 is currently produced using nitrogen from the air and H_2 sourced from fossil fuels. However, there is potential for NH_3 to be produced using H_2 from renewable energy sources or through direct photo-catalytic synthesis [1, 2]. Both are active areas of research and could potentially create zero-carbon fuel cycles using production, transportation, and conversion technologies that are very similar to those already in widespread use. However NH_3 also has its own challenges that need to be overcome. In order to better understand how well NH_3 and H_2 would perform as fuels, it is essential to understand their fundamental combustion properties and behavior.

Table 1: Comparison of properties of H_2, NH_3, and CH_4 relevant to combustion and storage.[3–7]

Properties	**Hydrogen (H_2)**	**Ammonia (NH_3)**	**Methane(CH_4)**
Boiling Point at 1 atm (K)	20.28	239.8	111.6
Typical storage pressure at 298 K (MPa)	69	0.99	25
Density at storage pressure (kg/m^3)	39	600	215
Gravimetric Energy Density (MJ/kg)	120	18.6	55.5
Volumetric energy density (MJ/L)	4.5	12.7	9
Minimum Ignition Energy (mJ)	0.011	8	0.28
Max. Laminar Burning Velocity (cm/s)	293.3	7	37.4
Lean Flammability Limit (Φ)	0.1	0.63	0.43

1.1 Ammonia-Hydrogen blends as fuels

While NH_3 has some of the aforementioned advantages, one the major challenges is its low flammability. It has a high minimum ignition energy (MIE), which makes it more difficult to ignite than most current fuels. Its volumetric heat release rate and laminar burning velocity (LBV) are both lower than most other fuels. Similarly, the lean flammability limit (LFL) is also significantly higher for pure NH_3 mixtures [8]. One way of improving these properties is by blending NH_3 with other fuels. NH_3 has been blended with hydrocarbons as well as H_2. H_2 is an attractive option since it is also devoid of carbon atoms, has a very low MIE, and a very high LBV compared to most other fuels. These characteristics of H_2 create safety issues and mechanical challenges when used on its own; however, blending it with NH_3 allows for some mitigation of these problems. Furthermore, mixtures with optimum or target values for desired properties can be created through blending, which is not possible with pure H_2 or NH_3 air-fuel mixtures. This motivates a deeper understanding of the fundamental properties of combustion for the various compositions possible with these two fuels. One such important property is combustion instability, which has a direct bearing on the operation of a system using the fuel and the LBV of the mixture, as well as storage and transportation safety concerns.

1.2 Combustion Instabilities

A fluid flow in which a small disturbance/perturbation results in a noticeable change in properties of the fluid flow (e.g. pressure, velocity) is considered to be unstable. They are fairly common in combustion and often manifest as pressure oscillations with growing amplitudes. They can become large enough to destabilize/extinguish the flame, or create oscillations in the overall system that can cause damage or malfunction, such as generating unsteady thrust or power. H_2 specifically is highly susceptible to combustion instabilities [9]. Combustion instabilities are often broadly categorized into three classes: intrinsic, chamber, and system instabilities[10]. Intrinsic instabilities are those that develop regardless of the combustion chamber and system. They are intrinsic to the mixture and conditions. Chamber instabilities are related to the combustion chamber and influenced by the shape and dimensions of the combustion chamber. They often feed off fluctuations in pressure and heat release caused by intrinsic instabilities. System instabilities in the overall system develop due to the interaction of chamber instabilities with other parts of the system. Intrinsic instabilities are the most relevant class to study when considering a mixture without taking into account its target system. Intrinsic instabilities experienced by premixed gaseous mixtures include body-force instability, thermal-diffusive instability, and hydrodynamic instability (also known as Darrieus–Landau instability) [11]. Body force instability is due to the fact that the flame front divides two regions of different densities, resulting in a situation similar to a less dense fluid resting below a higher density fluid, which is unstable. Diffusive-thermal instabilities are caused by the effect of flame-front curvature on the diffusion rates of heat released and the reactive species of the combustion reaction. Any disturbance that causes the front to bulge toward the unburned gas defocuses the heat flux towards the mixture. In the same way, it results in focusing the diffusive flux of the deficient reactant into the flame. If the thermal diffusivity of the mixture and the mass diffusivity of the limiting reactant are equal (the ratio of both is called the Lewis number L_e), then these effects balance so that the burning velocity is unaltered. For mixtures with Lewis numbers less than about unity, this mechanism is destabilizing. Finally, hydrodynamic instabilities exist because an interface between two fluids of different densities is unstable to any perturbation as one fluid expands into another. In the case of combustion, this interface is the flame front between the burned products and the unburned reactants. Practically, the forces that cause both diffusive-thermal and hydrodynamic instabilities exist at almost all times in a flame, however they can offset each other (as in the case of stable flames) or one may dominate the other, depending on the conditions.

The intrinsic instabilities of a mixture are important to understand as they contribute to chamber and system instabilities that affect the operation of the overall system. A constant volume combustion chamber (CVCC) is commonly used to study properties of a combustible mixture [12], often by studying the spherically expanding flame of the mixture of interest. A CVCC with optical access can be used with high-speed imaging to capture the visual features of such a flame [13]. Intrinsic instabilities appear as wrinkles on the surface of a spherically expanding flame that can develop cellular structures [13]. While instabilities have been quantified in terms of pressure oscillations and vibrations [14, 15], image processing methods have also been used [16], including spherically expanding flames for wrinkles and cells [17]. Several metrics have been used in the literature to quantify these visible instabilities, such as number of cells, cell density, and crack length [9, 13, 17, 18]. This study also uses an image processing method to detect and quantify the cracks/wrinkles in spherical NH_3-H_2 flame images. The images are captured from a CVCC by a Z-type Schlieren imaging setup with a high-speed camera. The NH_3-H_2 flame experiments were

conducted over a range of equivalence ratios as well as NH_3-H_2 blends. The following sections of this paper detail the experimental setup and the image processing methods used to study the cracks in the flame front.

2. Methodology

NH_3 and H_2 can be combined in different combinations in a fuel-air mixture. Similarly, there can be different equivalence ratios (Φ) of each NH_3-H_2 combination. The images used in this text are from a study which considered mixtures where H_2 ranges from 0% to 50% of the NH_3-H_2 fuel fraction (in increments of 10%). Each combination was then part of air-fuel mixtures where the equivalence ratios were 0.5, 0.7, 0.9, 1.0, 1.1, and 1.3. This adds up to a total of 36 mixture compositions. A CVCC combined with a data acquisition setup and a Schlieren with high speed camera was used to study these mixtures. The mixtures were prepared using the partial pressure method, allowed to mix for 3 minutes, and then ignited. The pressure data and high-speed images were recorded for analysis. Three trials were conducted in this manner for each of the 36 mixtures. The overall setup is the same as detailed in prior publications [19–22]. The schematic for the overall experimental setup is shown in Figure 1 and a 3D rendering of the CVCC is shown in Figure 2.

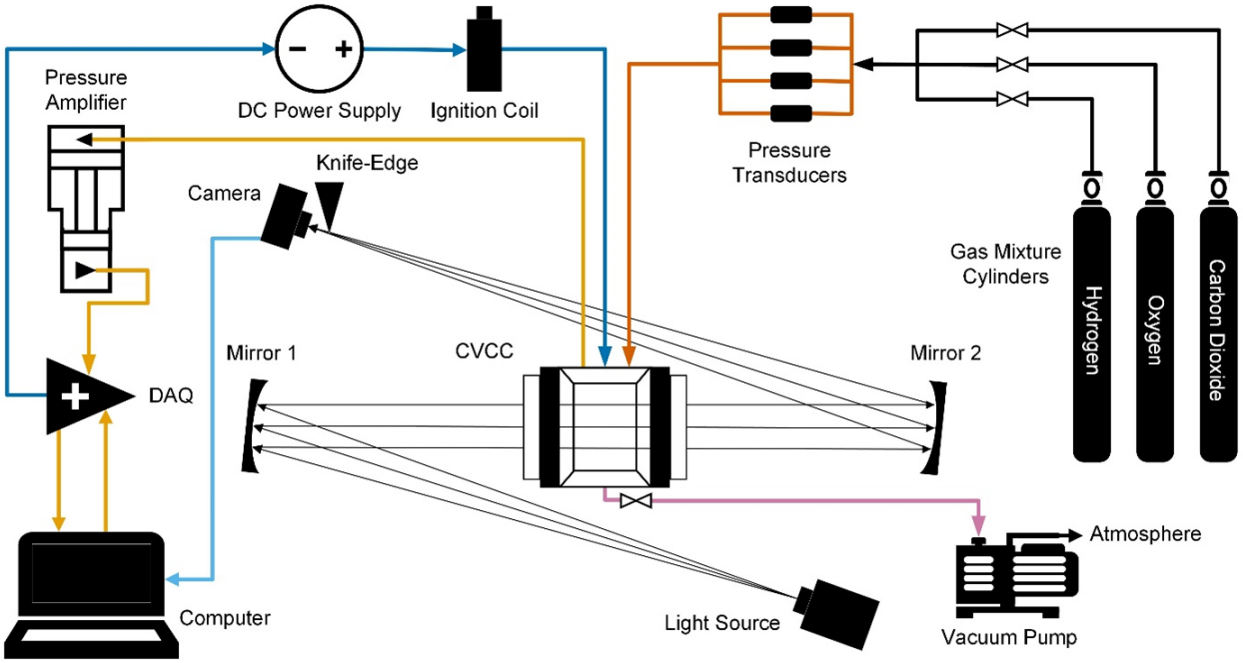

Figure 1: Schematic diagram of the experimental setup. Mixtures in the CVCC were ignited via a computer, which also acquired pressure data and triggered a high-speed camera to capture the flame images via Z-type Schlieren imaging.

The videos obtained from these experiments are the primary object of study in this paper. The 384x384 resolution images were obtained at 8000 frames per second. The image analysis was done using OpenCV[23] through Python. Processing Schlieren images can be challenging in some ways compared to other imaging methods such as shadowgraphs. The intensity of pixels of cracks

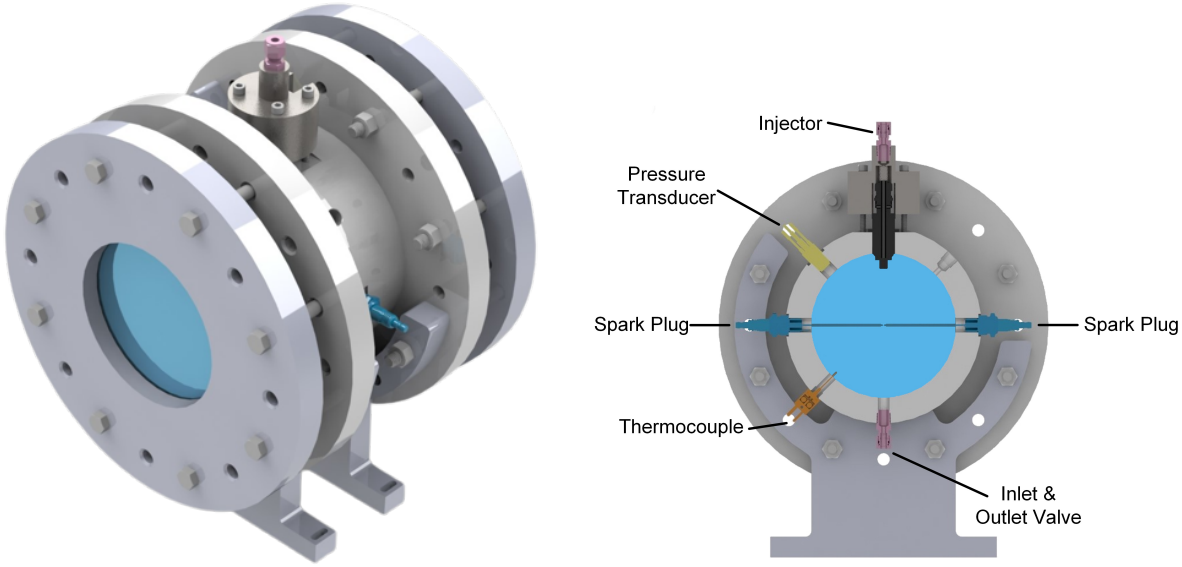

Figure 2: Isometric view of the Constant Volume Combustion Chamber (left) and a cross-section indicating the different components (right)

or edges can vary greatly depending on the position in the image. This means thresholding cannot be used to make features such as cracks and edges more prominent. This makes the use of edge detection methods that utilize gradients necessary (such as Canny). The process started by taking a background frame from the video (before ignition) and extracting the features of the chamber (electrodes extending from spark plugs, chamber walls, and injector). This was done using the Canny edge detection algorithm[24] (as implemented in OpenCV) followed by finding the contour which represents all of the chamber's features. The contour was used to mask out these features from the subsequent frames. All steps after this initial procedure were repeated for all frames. There were two copies of each frame, a "flame masking frame" used to detect the flame front and an "edge frame" to detect cracks as edges. Canny edge detection was applied to the flame masking frame, followed by the background mask to eliminate the background elements. The edges in this masked image then underwent morphological closing. The built-in OpenCV contour finding function was used on this image to detect the flame front. This flame front contour was used to create the eponymous mask in the frame.

The "edge frame" was subjected to bilateral filtering to clear out noise without any significant effect on edges. This was followed by a sharpening filter to make the cracks in the flame more prominent. Canny edge detection was used on this filtered frame to detect all edges in the frame, turning it into a binary image in the process. This edge-detected, binary image was then masked by the background mask (to remove the chamber features) and then the flame front mask from the flame masking frame to remove the flame front as well as any edges due to noise outside the flame front. This meant that the remaining detected edges were all due to cracks. Morphological closing and erosion operations were applied on these edges to complete any gaps in cracks missed during edge detection and remove any extra thickness obtained during this process. Due to erosion, the only remaining white pixels at this point would be the lines running through the cracks' center and

the number of non-zero pixels could be used to approximate the length of cracks in pixels. The radius of the flame was calculated from its circumference. This entire process is summarized in Figure 3 and resulted in cracks being detected such as those shown in Figure 4. Crack lengths were used to quantify instabilities instead of the number of cells and cell density, as there were several conditions with cracks that did not develop complete cellular structures.

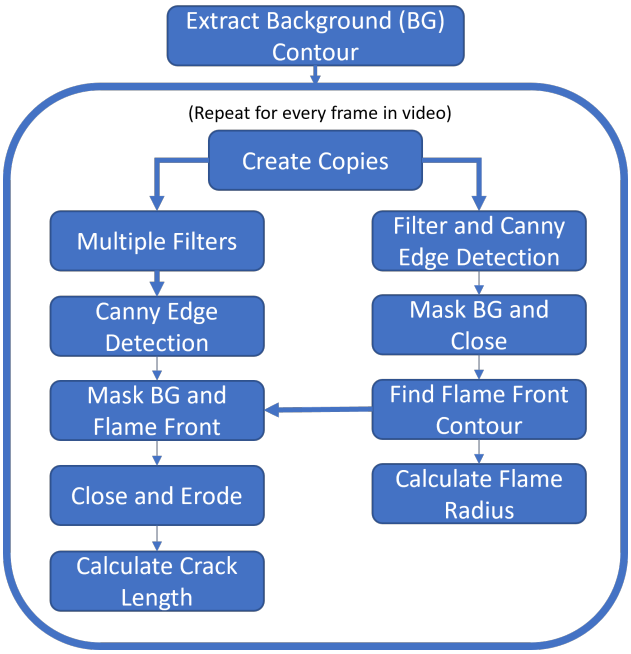

Figure 3: Flow chart of image processing algorithm for crack detection and measurement

However, it was observed that the detected cracks were thicker than 1 pixel in practice, despite the morphological erosion operations. This was due to the fact that thicker cracks were detected as two separate edges and the ensuing closing operation closed them into one thick structure. The subsequent erosion operations reduced them to some extent, but some thick cracks remained. So the lengths were adjusted based on comparison with some manual measurements and then converted into centimeters using the calibration factor for the imaging setup (0.04 cm/pixel). This gives a quantitative measure in terms of units of length and is a valid representation of the extent of instabilities in a given image of spherically expanding flames. However, considering the relatively crude nature of the adjustments, it is necessary to note that the lengths reported by this image processing methodology are still not exact physical lengths of the cracks on the surface of the spherical flame. This means the use of length of cracks mentioned here to compare instabilities between different conditions is only valid between images and videos using the same code. Furthermore, the cracks appear flat in the images, but in reality are on a spherical surface. Their exact lengths would come from translating the detected cracks onto spherical surfaces of the calculated radii.

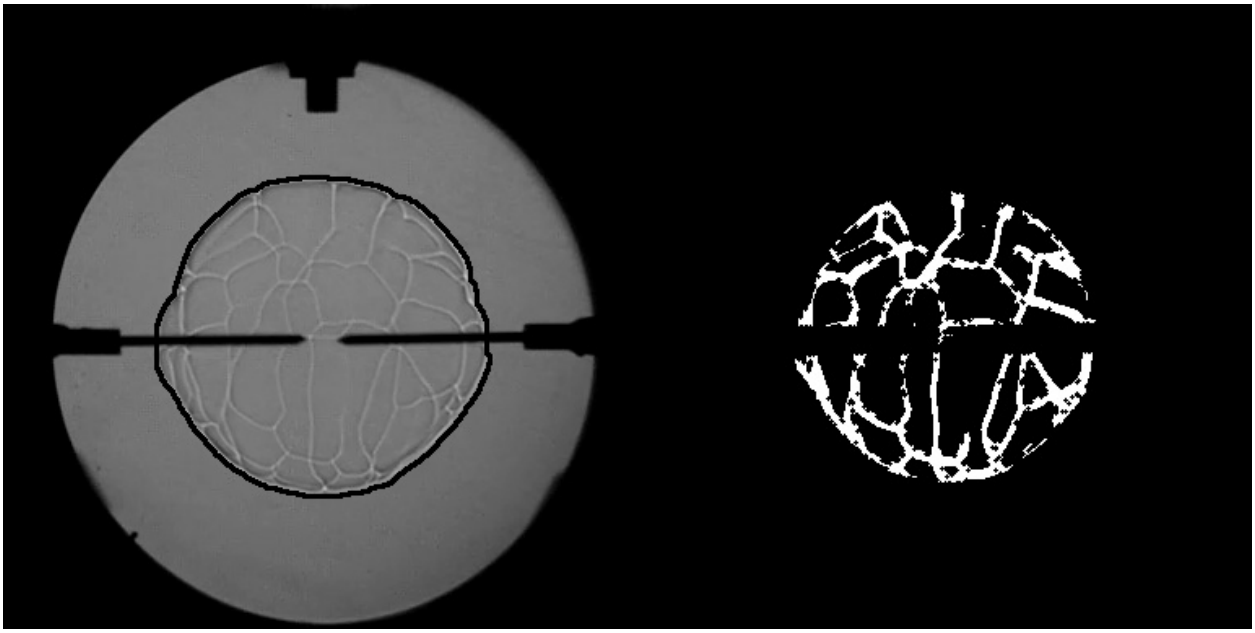

Figure 4: Example of Schlieren image with the flame front contour and the corresponding crack detected image ($\Phi = 0.7$, H_2 = 40%)

3. Results and Discussion

The crack lengths were obtained for each frame of all videos. All frames with multiple contours in the flame front frame were discarded as that indicated something other than the flame front had also been detected as a contour. Also, images with the flame radii below 1 cm and above 4.8 cm were not considered in order to avoid images where the spherical flames hadn't developed yet as well as those where the flame was large enough to start interacting with the chamber. Not considering the conditions where there was no flame ($\Phi = 0.5$ with $\%H_2 = 0$ and 10) or the trials where captured videos were not suitable (due to improper lighting or partial obstructions in the line of sight of the camera), this resulted in a total of 86 trials with usable videos across 34 conditions. The resulting data indicated the evolution of cracks/wrinkles vis-a-vis crack length in the flame front. The number of cracks detected in each frame as the flame developed is illustrated for a case with a significant length of cracks and no cracks in (Figure 5).

It was observed that for a given equivalence ratio, the maximum number of cracks observed increases with the increase in H_2 content of the mixture. This pattern is clearly illustrated by Figure 6, which shows the maximum crack length in cm across the range of equivalence ratios and percentage of H_2 in the fuel volume fraction of the mixture.

The maximum crack length shown in Figure 6 is an average of three trials for each condition. A more important pattern apparent here is that as the mixture becomes richer, the maximum number of cracks becomes lesser and lesser even at higher fractions of H_2. This implies that more H_2 can be added to the mixture without instigating instabilities at stoichiometric and richer conditions than at leaner conditions. This could have consequences for choosing regions of operation for an NH_3-H_2 system, if the extent of intrinsic instabilities are critical to the operation. This becomes especially important considering the fact that other factors such as emissions, heat release

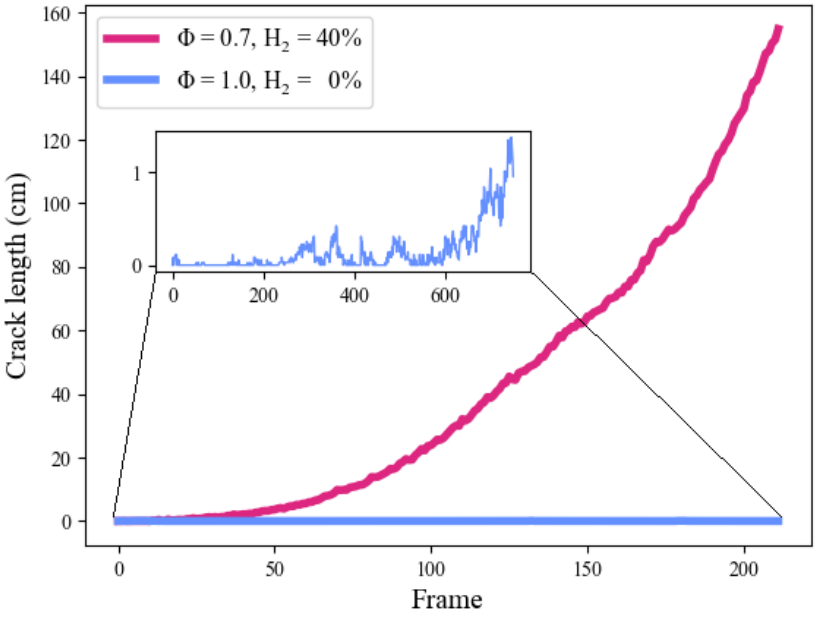

Figure 5: Evolution of cracks for cases with numerous cracks ($\Phi = 0.7$, H_2 = 40%), and No cracks ($\Phi = 1.0$, H_2=0%)

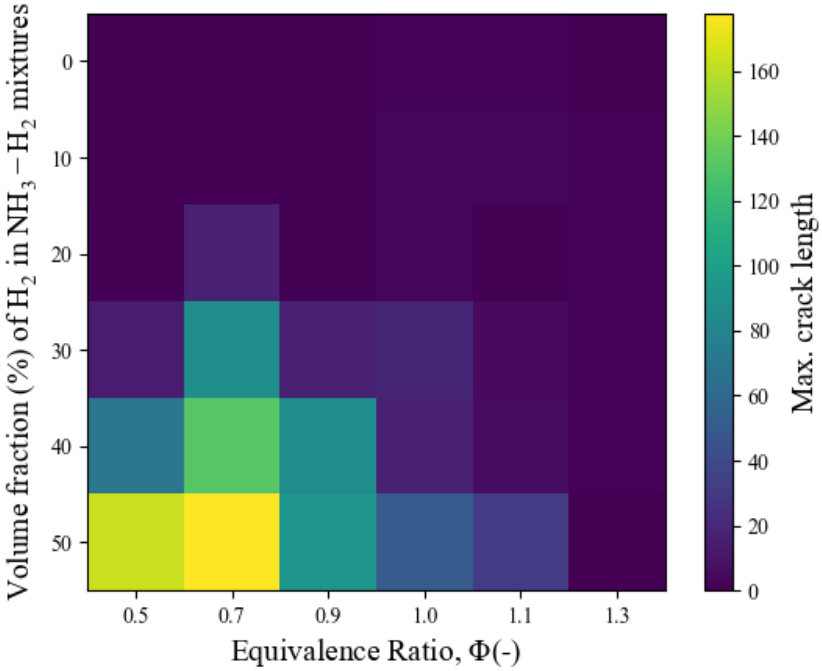

Figure 6: Heatmap showing the maximum crack length detected for each equivalence ratio and blend combination

rate, and laminar burning velocities may also vary across the H_2 fractions and equivalence ratio combinations. The behavior itself is consistent with how pure H_2-air spherical flames behave as reported by [9]. Cracks in H_2 appear earlier and develop more quickly into cellular structures at lower equivalence ratios in pure H_2-air flames. Tinaut et al. attribute this to the change in Lewis number caused by the changing mass diffusivity of the deficient reactant, which is H_2 in leaner cases. This explains the behaviour observed in the NH_3-H_2 blends here, as increasing the H_2 content increases its contribution to the mixture properties. So the maximum crack lengths as well as the speed at which they evolve increase with the fraction of H_2 in the mixture and this behaviour is more pronounced at lower equivalence ratios.

4. Conclusions

Schlieren images of spherically expanding flames of NH_3-H_2 blends in a CVCC were analyzed for cracks/wrinkles using image processing. It was observed that the maximum length of cracks, as well as speed at which they develop, increases with an increase in H_2 content in the mixture. The tendency to develop cracks is higher at lower equivalence ratios because of the non-unity Lewis number caused by H_2 as the deficient reactant at leaner conditions. This means that systems sensitive to intrinsic instabilities might have to avoid leaner conditions at higher concentrations of H_2 in NH_3-H_2 blends used as fuels. There are several directions in which this work can be extended. Firstly, there is potential for the image processing methodology described here to be improved to detect crack lengths more accurately and be extended to calculate cells and cell density for cases where cellular structures develop. Furthermore, neural network based methods (such as Convolutional Neural Networks, CNNs) may provide potential improvements in performance and robustness against imperfect and noisy images. It would also be valuable to study the effect of the instabilities observed here on the performance of practical systems such as burners, turbines and IC engines.

5. Acknowledgements

This work relates to Department of Navy award N00014-22-1-2001 issued by the Office of Naval Research. Additional support for the corresponding author provided by the Fulbright Foreign Student Program.

References

[1] S. Zhang, Y. Zhao, R. Shi, G. I. Waterhouse, and T. Zhang, Photocatalytic ammonia synthesis: Recent progress and future, EnergyChem 1 (2019) 100013. DOI: https://doi.org/10.1016/j.enchem.2019.100013.

[2] R. Lan, J. T. S. Irvine, and S. Tao, Synthesis of ammonia directly from air and water at ambient temperature and pressure, Scientific Reports 3 (2013) 1145. DOI: 10.1038/srep01145.

[3] M. Aziz, A. T. Wijayanta, and A. B. D. Nandiyanto, Ammonia as Effective Hydrogen Storage: A Review on Production, Storage and Utilization, Energies 13 (2020), DOI: 10.3390/en13123062.

[4] H. Haase, Electrostatic hazards: their evaluation and control, 1. Aufl, Verlag Chemie, Weinheim ; New York, 1976, 124 pp.

[5] F. Verkamp, M. Hardin, and J. Williams, Ammonia combustion properties and performance in gas-turbine burners, Symposium (International) on Combustion 11 (1967) 985–992. DOI: https://doi.org/10.1016/S0082-0784(67)80225-X.

[6] A. Hayakawa, T. Goto, R. Mimoto, Y. Arakawa, T. Kudo, and H. Kobayashi, Laminar burning velocity and Markstein length of ammonia/air premixed flames at various pressures, Fuel 159 (2015) 98–106. DOI: https://doi.org/10.1016/j.fuel.2015.06.070.

[7] K. Mazloomi and C. Gomes, Hydrogen as an energy carrier: Prospects and challenges, Renewable and Sustainable Energy Reviews 16 (2012) 3024–3033. DOI: https://doi.org/10.1016/j.rser.2012.02.028.

[8] J. N. Klüssmann, L. R. Ekknud, A. Ivarsson, and J. Schramm, *Special report on Ammonia Applications in IC Engines*, IEA-AMF, 2020, URL: https://www.iea-amf.org/content/fuel_information/ammonia (visited on 11/29/2022).

[9] F. Tinaut, M. Reyes, A. Melgar, and B. Giménez, Optical characterization of hydrogen-air laminar combustion under cellularity conditions, International Journal of Hydrogen Energy 44 (2019) 12857–12871. DOI: 10.1016/j.ijhydene.2018.11.134.

[10] M. Barrère and F. Williams, Comparison of combustion instabilities found in various types of combustion chambers, Symposium (International) on Combustion 12 (1969) 169–181. DOI: https://doi.org/10.1016/S0082-0784(69)80401-7.

[11] F. A. Williams, Combustion Theory: The Fundamental Theory of Chemically Reacting Flow Systems, en, 2nd ed., CRC Press, 1985, DOI: 10.1201/9780429494055.

[12] T. W. Ryan and T. J. Callahan, Engine and Constant Volume Bomb Studies of Diesel Ignition and Combustion, SAE Transactions 97 (1988) 756–764, URL: http://www.jstor.org/stable/44471572 (visited on 01/17/2023).

[13] F. Wu, G. Jomaas, and C. K. Law, An experimental investigation on self-acceleration of cellular spherical flames, Proceedings of the Combustion Institute 34 (2013) 937–945. DOI: 10.1016/j.proci.2012.05.068.

[14] T. Kobayashi, S. Murayama, T. Hachijo, and H. Gotoda, Early Detection of Thermoacoustic Combustion Instability Using a Methodology Combining Complex Networks and Machine Learning, Physical Review Applied 11 (2019) 064034. DOI: 10.1103/PhysRevApplied.11.064034.

[15] U. Sengupta, C. Rasmussen, and M. Juniper, Bayesian Machine Learning for the Prognosis of Combustion Instabilities from Noise, (2020), DOI: 10.17863/CAM.50130.

[16] O. Choi, J. Choi, N. Kim, and M. C. Lee, Combustion Instability Monitoring through Deep-Learning-Based Classification of Sequential High-Speed Flame Images, Electronics 9 (2020) 848. DOI: 10.3390/electronics9050848.

[17] S. Huang, Y. Zhang, R. Huang, S. Xu, Y. Ma, Z. Wang, and X. Zhang, Quantitative characterization of crack and cell's morphological evolution in premixed expanding spherical flames, Energy 171 (2019) 161–169. DOI: 10.1016/j.energy.2018.12.202.

[18] M. Reyes, R. Sastre, F. Tinaut, and J. Rodríguez-Fernández, Study and characterization of the instabilities generated in expanding spherical flames of hydrogen/methane/air mixtures, International Journal of Hydrogen Energy 47 (2022) 22616–22632. DOI: 10.1016/j.ijhydene.2022.05.063.

[19] M. Morovatiyan, M. Shahsavan, J. Aguilar, M. Baghirzade, and J. H. Mack, An assessment of hydrogen addition to methane combustion with Argon as a working fluid in a constant volume combustion chamber, Combustion Science and Technology 194 (2022) 2395–2413. DOI: https://doi.org/10.1080/00102202.2020.1870454.

[20] M. Morovatiyan, M. Shahsavan, M. Baghirzade, and J. H. Mack, Impact of syngas addition to methane on laminar burning velocity, Journal of Engineering for Gas Turbines and Power 143 (2021), DOI: https://doi.org/10.1115/1.4049012.

[21] M. Baghirzade, M. N. Nasim, B. Nawaz, J. Aguilar, M. Shahsavan, M. Morovatiyan, and J. H. Mack, Analysis of Premixed Laminar Combustion of Methane With Noble Gases as a Working Fluid, ASME 2021 Internal Combustion Engine Division Fall Technical Conference American Society of Mechanical Engineers, (2021), V001T04A005, DOI: 10.1115/ICEF2021-67516.

[22] M. Morovatiyan, M. Shahsavan, J. Aguilar, and J. H. Mack, Effect of argon concentration on laminar burning velocity and flame speed of hydrogen mixtures in a constant volume combustion chamber, Journal of Energy Resources Technology 143 (2021), DOI: https://doi.org/10.1115/1.4048019.

[23] G. Bradski, The OpenCV Library, Dr. Dobb's Journal of Software Tools (2000).

[24] J. Canny, A Computational Approach to Edge Detection, IEEE Transactions on Pattern Analysis and Machine Intelligence PAMI-8 (1986) 679–698. DOI: 10.1109/TPAMI.1986.4767851.